Electrical Performance Evolution and Fatigue Mechanisms of Silver-Filled Polymer Ink Under Uniaxial Cyclic Stretch

Gabe Cahn[1], Olivier Pierron[1,*] and Antonia Antoniou[1,*]

[1] The G.W. Woodruff School of Mechanical Engineering

Georgia Institute of Technology, Atlanta, GA, 30332-0405, USA

[*]Corresponding authors: olivier.pierron@me.gatech.edu and antonia.antoniou@me.gatech.edu

Abstract

Flexible hybrid electronics rely upon compliant interconnects in order to maintain performance integrity in cases that require repeated elongation, including repeated stretching. A class of such conductive interconnects are composites of polymer with conductive particles that can be stretched at high strains without circuit failure. However, their fatigue response has so far remained largely unexplored and is essential prior to using in health monitoring applications. In this research, a stretchable silver-filled conductor is evaluated under high-strain cycling. In-situ techniques, including 4-point resistance measurement and laser profilometry, are used to correlate changes in electrical performance to the fatigue response. Surface crack formation is extensive upon stretching during the first loading cycle, forming a heavily interconnected crack network at higher strains that does not immediately result in open circuit failure. Resistance increase with cycling is attributed to a gradual deepening of these cracks until their depths approach the film thickness, eventually leading to electrical failure. Fatigue life, the number of cycles required to reach a predetermined electrical performance limit, is shown to be most influenced by the applied strain amplitude. Using a normalized resistance increase limit of

R/R_0=500, it is found that 500 μm wide conductive lines endure 23 cycles at 35% strain amplitude, but this becomes over 500 cycles when the amplitude is dropped to 5%. Sensitivity to mean strain, ε_m, is relevant to strain amplitudes below 15%. In this manner, a composite conductor was shown to exhibit crack evolution behavior distinctly different from homogeneous metallic films.

Introduction

Flexible hybrid electronics integrate compliant circuitry with CMOS-based chip components to yield functional devices that can stretch, and conform to curved surfaces. A common method of producing flexible electronic systems is to print thin conductive traces onto flexible substrates such as polymers, paper, and textiles. This opens opportunities for a host of new applications, while offering advantages of portability, reductions in cost, size, and weight, as well as replacement of bulky wire harnesses and assemblies. Such applications require electronics to operate effectively after, and often during, exposure to high strain (for example, up to 30% for wearable applications) (1).

Several types of compliant conductors (2-4) are in development to satisfy strain requirements, each with mechanical limitations. For example, one drawback of using thin metallic films as the conductor is their substantial elastic property mismatch with the polymer substrate, often leading to early degradation of the electrical behavior due to cracking (5-15). These conductors are therefore limited to bendable electronic applications, where the maximum strains do not exceed a few percent. Common applications for metal thin films include solar cells (16), energy harvesting devices (17), RFID antennas (18), health monitors (19), and other sensors (20-22).

In order to enable stretchable applications, alternative conductive thin films are being explored(23). Most common conductors for stretchable applications are composite films made of conductive metallic filler particles in a polymer matrix (binder) (24-26). At a certain filler volume fraction threshold, the conductive particles form a cohesive percolation network, across which current can flow. Such composite materials have shown promise as electrical interconnects for their higher tolerance of applied strain when printed as inks onto polymer substrates (27). Inclusions have ranged across PZT powders (28, 29), carbon black (30, 31), CNTs (32-35), and silver flakes (36, 37) , among others.

Researchers have successfully demonstrated continuous electrical conductivity of silver flake filled polymer composite inks when subjected to strains upward of 600% (38), though the resistance increases with applied strain. First order approximations and models (39) have been used to predict electrical performance in such hybrid conductors. They assume uniform distribution of filler material, as well as uniform deformation. These models agree with experimental data for low applied strain (<<5%) (26, 40). Higher order models have also been created to incorporate agglomeration and deformation of inclusions (41-43) at larger applied strains under the assumption that there are no other inherent defects introduced in the inks that can limit conductivity.

A prior study explored the electrical response of commercially available composite conductive thin films on polymer substrates under monotonic stretch(44). It examined composite thin films that had the same silver flake type and nearly identical flake fraction but different polymer matrix (with different moduli) and found the resistance increase to be different than model predictions. That study found two distinct deformation mechanisms during stretching: localized necking and

localized surface crack formation. It was found that the conductive composite thin films with lower matrix modulus formed multiple surface cracks with applied stretching. While the flake fraction remained nearly invariant close to the crack tip, there was still an increase in resistance with stretching. The resistance increase was attributed to a decrease in the thin film conductive cross-sectional area with surface crack formation. The appearance of such defects as cracks, and localized necks is a key difference from prior models. That recent work reported that conductive inclusions remained undeformed and unagglomerated even at high applied strains, a difference from prior models. Overall, the inks with lower matrix modulus had better resistance evolution with stretching despite pre-existing voids and despite forming surface cracks.

The electrical behavior of compliant conductors under cyclic loading is an important design parameter since ink reliability under repeated loading is expected in medical or structural applications. Common studies that explore conductive composite films' electrical response to fatigue(45-49) correlate in situ resistance measurements to external processing and testing parameters such as thickness of the supporting substrate, resolution of conductive print lines, applied strain amplitudes, and the manner in which strains are applied (e.g. bend vs stretch). Few explore internal deformation mechanisms and electrical measurements under cyclic loading (50). This study generates strain life curves over the full range of applied strains for such inks: essential knowledge for designers of health and structural monitoring devices. Moreover, it provides a fundamental understanding of the progression of localized damage under cyclic loading that is different from prior knowledge due to only conductive particle deformation. This manuscript summarizes such a study, which uses in situ strain mapping of topographical features to monitor deformation, along with concurrent electrical measurements, on commercially conductive

composite thin films with silver flakes and a lower matrix modulus. As mentioned before, pre-existing voids are present in this ink but they were not as detrimental to electrical performance under monotonic loading. Indeed, a properly calibrated void architecture may delay crack nucleation, and also attenuate damage propagation through crack tip blunting and the annihilation of dislocations. This has been observed in nanoporous silver thin films, which showed improved electrical life in the fatigue regime (51). Nanohole patterning of Cu film has yielded similar benefits (52). Within filled polymer conductors, deformation of and collapse of pre-existing void space during elongation caused new surface contact which mitigated resistance increases(49).

The manuscript is organized as follows: the experimental protocol and characterization steps are described, followed by results and discussion.

Experimental Methodology

Sample Preparation

The flexible conductor used in this work is Dupont's PE 874(53), comprised of a polymer matrix with Ag flake inclusions loaded to a volume fraction of approximately 55%, as reported by the manufacturer. The matrix has a polyurethane binder, which is intended for compatibility with compliant substrates. The ink was screen printed onto TE-11C (54) thermoplastic polyurethane (TPU) sheets supported by a temperature stable carrier layer. Printing processes were performed on site by DuPont, and optimized for reliability of print design geometries, ink-substrate adhesion, and electrical characteristics.

A single pass print achieves nominal ink thickness between 8 and 10 µm, on top of the TPU substrate that measures approximately 89 µm thick once removed from the carrier. Print lines for this work include 0.5 mm, 1.0 mm, and 2.0 mm widths, as shown in Figure 1a. These are first printed onto larger sheets, and then individually cut along print boundary markers into 55 x 10mm samples for testing. In this study, 28 unique samples were tested in total for different trace widths, and fatigue testing parameters. The samples were cut with a circular blade along their print lines. The print design is such that samples can be tested in uniaxial tension, with contact pads for four-point resistance measurement. Along the length of the trace, tick marks are included to denote 2mm increments in the undeformed condition.

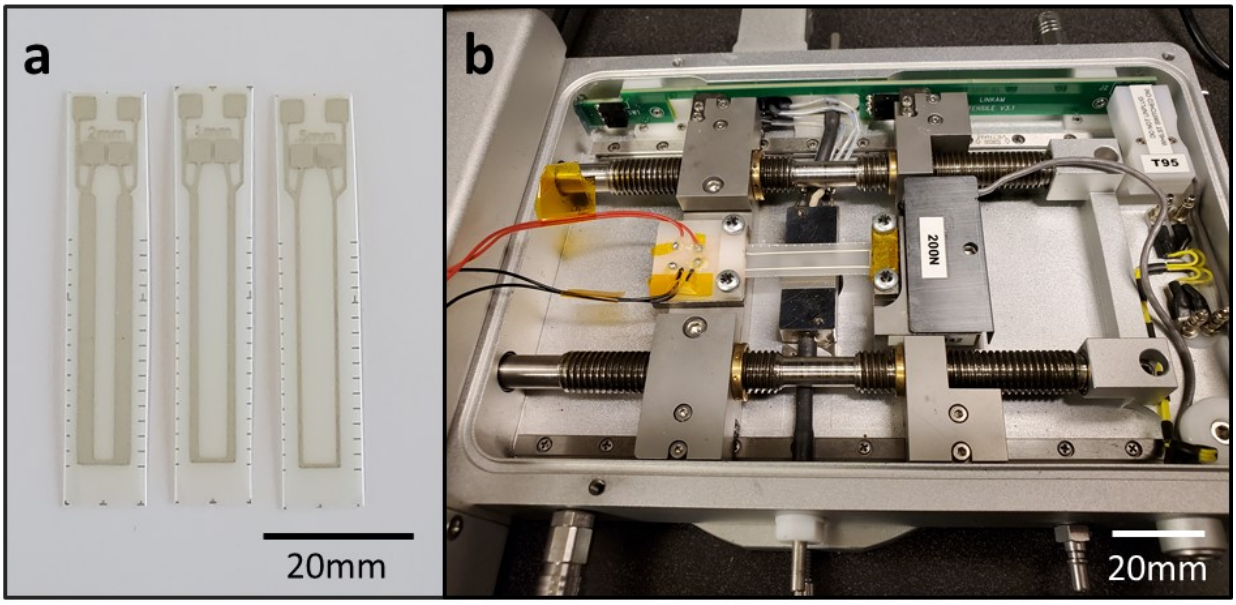

Figure 1. (a) Line width variations of PE874 ink screen printed onto TPU substrate (b) Sample loaded into Linkam TST350 micro tensile test stage, formatted for in-situ resistance and confocal microscopy measurements.

Mechanical and Electrical Measurements

For the experiments, sample strips are placed into a Linkam TST350 micro tensile test stage (55), as shown in Figure 1b. Clamps are used to isolate a 30 mm long initial working length in the unloaded specimen under test. One top clamp is made from non-conductive nylon, and was laser cut to facilitate four spring-loaded electrical contacts. These interface with the printed pads on the sample, and connect, via wire leads, to an Agilent 34401A digital multimeter. The remaining metallic clamp components are electrically isolated from the conductor line, either by the TPU substrate, or Kapton tape.

The testing protocol was as follows: the resistance changes were monitored in samples that were elongated by applying a maximum applied strain, ε_{max}, and then strain cycled between the ε_{max} and a minimum applied strain, ε_{min}, that was always greater than 0% strain (e.g. Tension-Tension cycling). Controlled parameters for any given test include strain rate (commonly 2% per second), strain amplitude: $(\varepsilon_{max}- \varepsilon_{min})/2$, and mean strain: $(\varepsilon_{max} + \varepsilon_{min})/2$. The Linkam stage outputs a displacement measured to the nearest 0.01mm (0.03% strain), along with load to a resolution of .001N, and timing to the nearest microsecond. Resistance measurements are output from the multimeter to the nearest milliohm. All equipment is synchronized and controlled via Labview script, which captures measurement data at a sampling rate of 2Hz. These values are subsequently used to calculate normalized resistance (R/R_0) for a given applied strain amplitude and mean strain during the test. Normalized resistance is specific to the sample section attached between the clamps so care was taken to properly measure dimensions of that segment. This was accomplished by taking the measured initial distances between clamps for each specimen to use as the baseline for applied strain calculations. Additionally, timestamps on collected data are used to correlate measurements and calculations to specific cycle increments. The normalized

resistance was plotted for different combinations of maximum and minimum applied strains (or strain amplitude and mean strain). Individual tests were halted once resistance measurements reached a consistent state of erratic values, or open circuit signals, such that further sampling no longer yielded coupled electrical and mechanical data.

In situ Confocal Microscopy Measurements

In order to observe the deformation of the conductive composite thin film, a select number of samples were tested with the Linkam stage while under an Olympus LEXT OLS4000 confocal microscope. This tool captures optical microscopy images, as well as information about the surface topography using the laser profilometer. The optical image is created by digitally stitching the field of view captures across a range of heights, thereby mitigating any compromise in image resolution from outside the depth of field of the optical objective. The laser scans give the topography of the view area and output the height measurements across the scanned area. Samples are scanned at a magnification that yields an area resolution of 0.25 μm per pixel in a 256 square μm window (1024 x 1024 pixels). Height measurement resolution is approximately 8.8 nm.

The conditions for the samples tested under the confocal microscope reflected the largest applied strain that could be applied while the normalized resistance under monotonic stretching remained less than 500. We note that there is no clear definition for fatigue life of thin films in the literature. Several criteria have been used, mainly related to an arbitrary increase in normalized resistance (from 2% to 25%) (8, 56). In our work, we define R/R_0=500 to be a parameter of interest based on our experimental results. Coincidentally, at a normalized

resistance of 500, unstable crack propagation has been observed during stretching of brittle thin oxide films deposited on a polymer substrate(57). For samples tested at a maximum applied strain of 80%, the Linkam stage was rotated so as to avoid collision with other objective lenses attached to the confocal microscope. The angle of rotation was measured before cycling. The test was paused for a few moments at maximum strain of 80% every 10 cycles to allow time to complete the scans, and finally ended after the completion of 100 total cycles.

The relative positioning of the sample underneath the LEXT microscope objective does not remain constant across every cycle set. As such, the profile scans cannot be compared directly with each other after each cycle. The height profiles need to be translated and possible interpolation is needed before comparing the thin film surface after each cycle. For this purpose, digital image correlation (DIC) is used, a scale agnostic method that monitors changes in features during loading using image registration. Specifically, we take all topographical images of the surface obtained using the LEXT microscope at different cycles and perform a comparison for each one of them with the topographical image obtained during the first cycle using DIC. The height profile contours have unique features as can be seen from Figure 2a contour and Figure 2b surface height profile of the surface. The topographical images are separated into smaller subsets whose radius, r_s, is 10 pixels, which equals to 5 μm.

Assuming deformation in each subset to be a linear, first order transformation, in-plane displacements u and v are analytically determined for each subregion center with sub-pixel resolution. The output gives in-plane translation of each topographical map after each cycle. Such a field can be generated to compare any cycle set increment. Figure 2c shows the surface after

100 cycles with Figure 2d showing the relative displacements (of the order of 25 µm) from the first cycle.

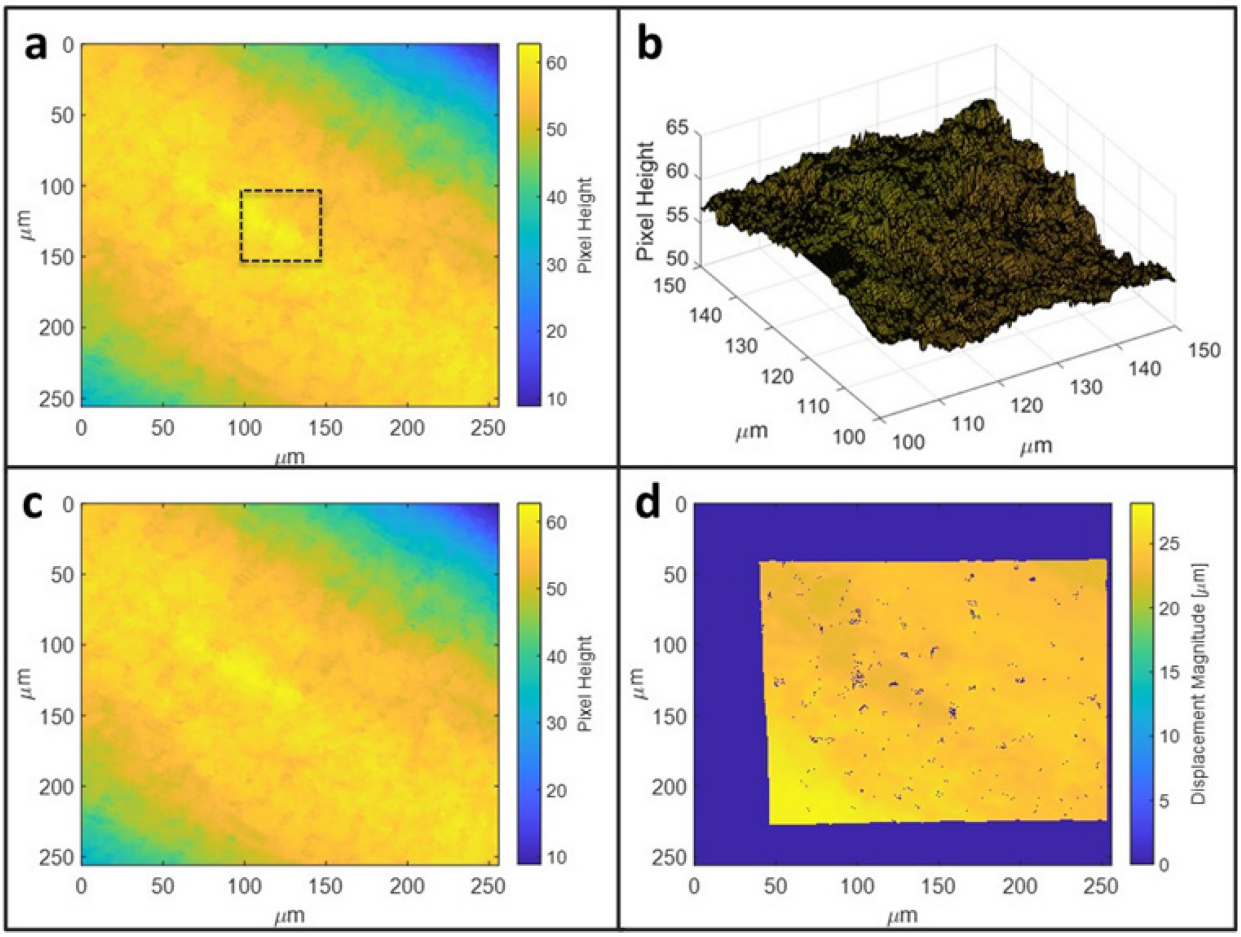

Figure 2. Topographical maps of a smaller region of the 0.5 mm PE874 print line (a) strained to 80%. The region within the dotted outline is selected for (b) 3D rendering. (c) 2D profilometry field of the same sample after cycling between 50% and 80% strain 100 times. (d) Translation map correlating the shift of the pre and post cycled sample scans seen in inserts (a) and (c). Note that the translation is nearly uniform with a magnitude of approximately 25 µm.

Results

The evolution of the heterogeneous conductive composite ink during monotonic stretching has been presented in a prior manuscript (44). For fatigue loading, during the first half cycle the conductive film will experience the same behavior as seen during the monotonic test. It is

therefore, worthwhile to describe the surface evolution and effect on resistance during such loading. Under monotonic stretch, the normalized resistance in PE 874 increases with applied strain. An example of this is presented by a single measured sample curve in Figure 3a. In-plane strain maps obtained by analyzing the surface evolution using Ncorr(58) revealed that there is strain localization that occurs very early in the loading. The localization is manifested in the form of surface cracks, captured from a different sample at varying strain increments and displayed in Figures 3b-e. The network of surface cracks does not penetrate through the thickness of the film, therefore maintaining some conductivity, although it is reduced from the unstretched configuration.

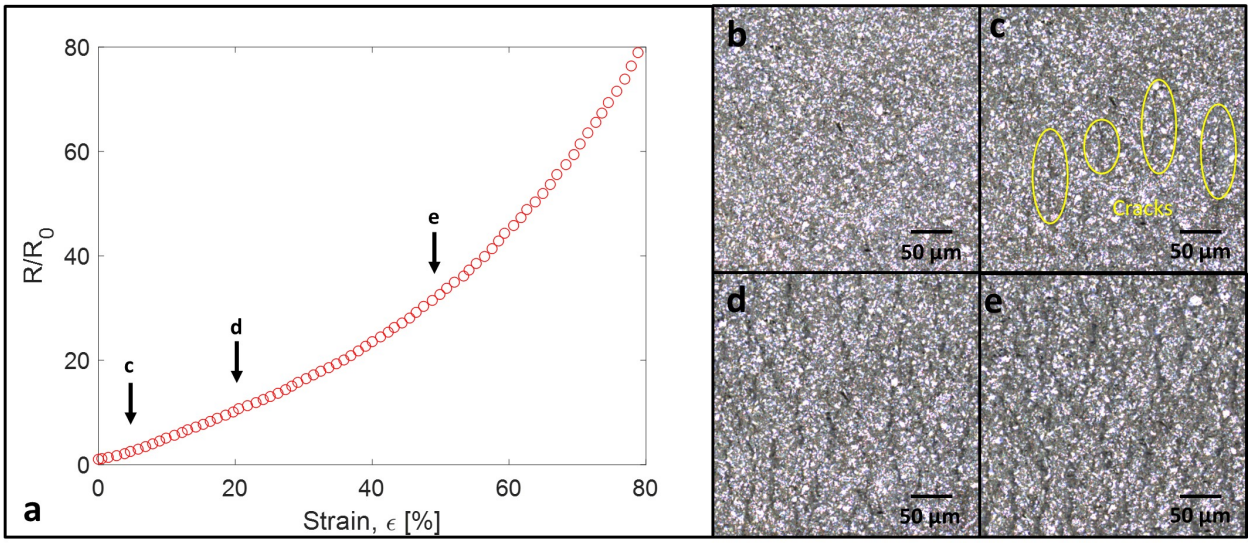

Figure 3. (a) Electrical Response to monotonic strain for 2mm wide PE 874 printed onto TPU (b) PE 874 in test stage, undeformed (c) PE 874 with 5% applied macro strain, surface cracking begins to be visible (d) PE 874 strain field for 20% applied macro strain (e) PE 874 with 50% applied macro strain.

During the first half cycle the resistance of the conductive print line increases while a network of surface cracks forms and becomes interconnected similar to what was observed in the monotonic test. As the applied strain decreases away from the peak strain value, the resistance decreases. However, under continuous cycling between two strain values, the relative resistance continues to increase from the initial (monotonic) values. Figure 4a illustrates the fatigue behavior for the first 30 cycles of a single 0.5mm sample elongated between 50% and 80% applied strain. The change in resistance is added to the initial measurement for the region being stretched, and normalized against this initial measurement. Figure 4b shows this same test continued to just under 150 cycles. At approximately 75 cycles, the resistance change behavior reaches an inflection point, where the relative difference between peak and valley resistance rises more rapidly and begins to become unstable. In many instances the measurement reads an open circuit near ε_{max}, and then returns to measurable levels at ε_{min}. This general trend is illustrated by the normalized resistance envelope outlined in red in the plot. The cyclic behavior is compared to that of a separate sample subjected to only the initial monotonic elongation and then held at ε_{max} for the duration of the test, as shown in green in Figure 4c. After a brief reduction in resistance, the electrical performance of the static sample remains constant. Therefore, strain cycling of samples leads to additional increase in resistance compared to a monotonic stretch and hold.

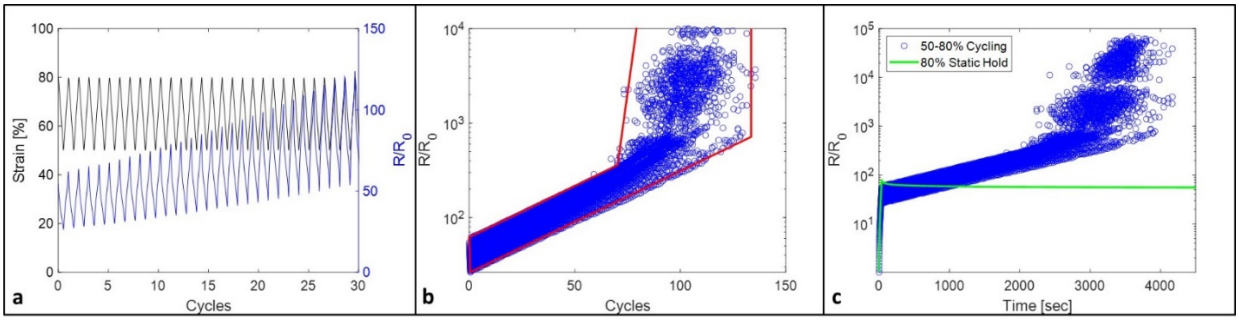

Figure 4. (a) First 30 cycles of 0.5mm wide PE874 print strained between 50% and 80% (strain range: 30%, mean strain: 65%. (b) Full trial data set for 0.5mm wide sample cycled between 50% and 80% strain. The red behavior envelope encompasses the majority of normalized resistance values, including open circuit measurements not seen in plot (c) 0.5mm wide sample cycled between 50% and 80% strain, inclusive of initial elongation from zero, superimposed by separate 0.5mm sample elongated to 80% and held at constant strain.

The failure limit, also known as fatigue life, N_f, is expressed as the number of strain cycles required to reach a designated performance threshold. Since the measured resistance for PE874 samples subjected to 80% strain is nearly 80 times the pre-strained value, a threshold of R/R_0=500 is selected for this work as the fatigue life performance limit. This becomes the unifying metric across all of the varied experimental case parameters, which include strain amplitude, mean strain, print line width, and strain rate. By mapping the fatigue life for each experiment, one can identify the parameters of strain cycling which hold the greatest influence over resistance change behavior.

Strain cycling was performed on 28 different sample prints for different conditions and summarized in Figure 5a-d. Figures 5a-b show significant influence of strain amplitude, ε_a , on cycle count to reach the normalized resistance limit, from 23 cycles at 35% to an average above 500 cycles at 5%. Furthermore, sensitivity to mean strain, ε_m, seems to depend on the strain amplitude. Above ε_a = 15%, the fatigue life does not appear to depend as much on mean strain. Below ε_a = 15%, the disparities become more significant. This is illustrated by the spread of failure points in Figure 5a, and the visible difference in slopes of the trend lines in Figure 5b. At ε_a = 10%, a mean strain of 65% yields failure around 50 cycles. This nearly quadruples to 190 cycles with a drop to 40% mean strain or less. When ε_a = 5%, a 75% mean strain fails after just over 300 cycles

but when the mean strain is 25% can extend the life to over 700. Trace width and strain amplitude are relevant parameters, but do not appear to significantly impact cycles to failure.

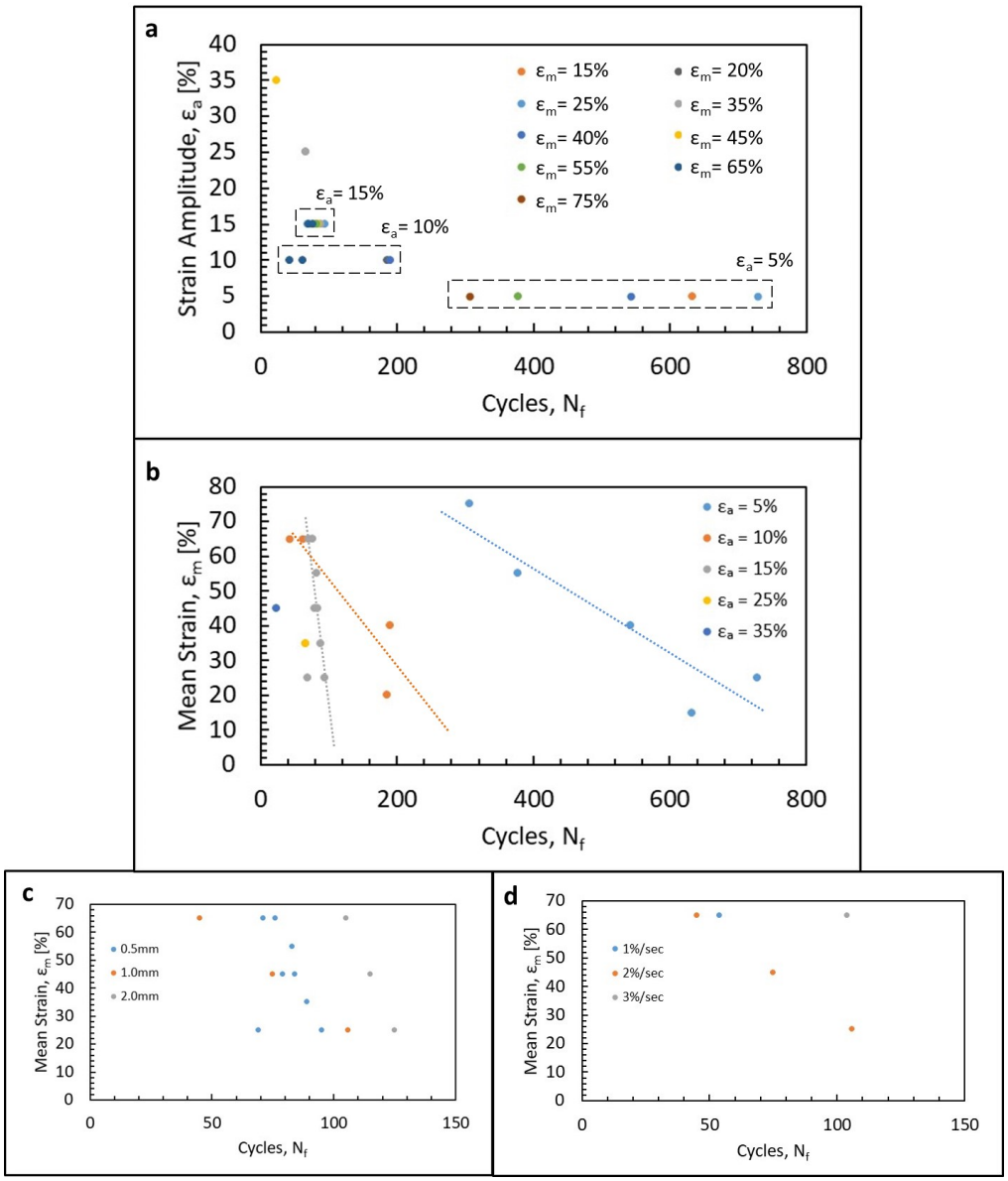

Figure 4. (a) Strain amplitude vs. cycles to $R/R_0 = 500$ for 0.5mm wide prints at 2%/sec strain rate. (b) Strain life for 0.5mm wide prints at 2%/sec strain rate. (c) Strain life for specimens subjected to 15% strain amplitude cycling at 2%/sec strain rate. (d) Strain life for 1.0mm wide prints subjected to 15% strain amplitude cycling at varying strain rates.

Figure 6 illustrates in-situ resistance measurements for a single 0.5mm wide print sample subjected to 100 cycles between 50% and 80% strain, with intermediate optical and laser profilometry scans every 10 cycles. The normalized resistance increases with cycling, as already shown in Figure 4. Between cycle sets, the normalized resistance is observed to decrease. Comparison of these two experiments clearly highlights that the general resistance increase behavior is the result of strain cycling, and not time-dependent effects.

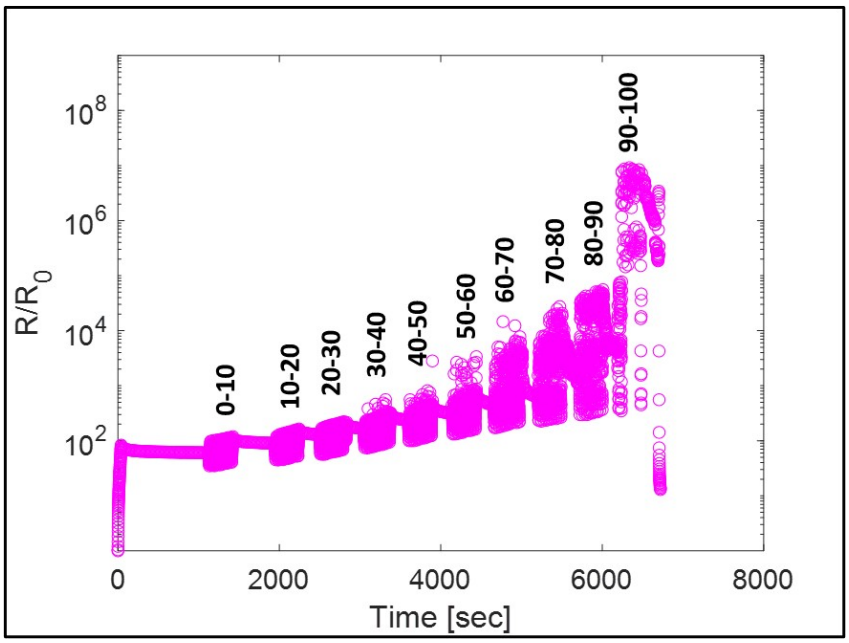

Figure 6. Normalized resistance behavior of 0.5mm print subjected to 100 cycles – in increments of 10 – of 50% to 80% strain, with intermediate optical and laser profilometry scans

A single 0.5mm wide print specimen in its unloaded state is displayed in Figure 7a. When elongated to 80% strain, but before cycling commences, a network of extensive cracks is already present (Figure 7b), similar to the one shown for the monotonic stretch in Figure 2. Dominant crack channels are roughly oriented perpendicular to the direction of elongation. The crack path is not a straight line, as might be seen in homogeneous metallic thin films, but by-passes around flakes. Due to the extensive cross-linking within the crack network, it is possible to trace pathways

that span the entire ink line. Note, also, that the width of the hybrid ink decreases with applied strain due to the Poisson effect. Figure 7c shows the same sample after the stage has been rotated approximately 34 degrees to avoid interference with the objective lenses of the microscope.

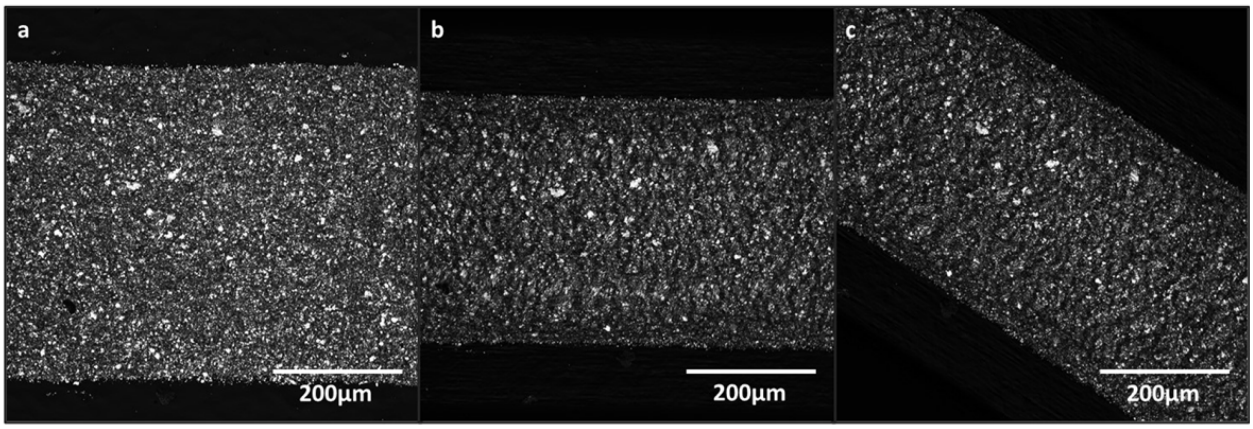

Figure 7. (a) 0.5mm wide print in unstrained condition. (b) 0.5mm wide print elongated to 80% strain. (c) 0.5mm print elongated to 80% strain, and rotated 34˚ to fit under confocal microscope.

Figure 8a shows a 256 µm square area of the 0.5mm PE874 print elongated to ε_{max} = 80%, but not yet cycled. Figure 8b shows the topographical image of the same approximate region following 100 strain cycles. The topographical features are compared using Ncorr and the resulting displacement of the features before and after cycling is obtained. Once the respective topographies are aligned the resulting change in height between uncycled and 100 times cycled sets is compared, revealing the height delta field in Figure 8c. These height differentials can be upwards of 8 µm, which is sufficient to penetrate the entire thickness of the ink print when the resistance approaches that of an open circuit. We note, that under a monotonic test and hold as seen in Fig. 4c, the ink network does not change during the hold. As a result, the resistance does

not increase but remain invariant with hold time. This was verified by comparing the topographical images of Fig. 7 after the initial 80% strain was applied but before the cycling test commenced.

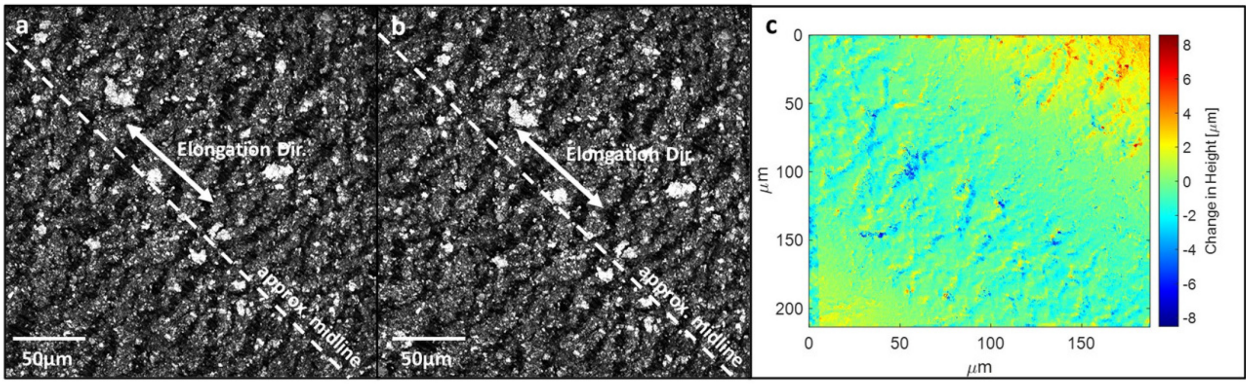

Figure 8. (a) 0.5mm print elongated to 80% strain, rotated, uncycled (b) 0.5mm print elongated to 80% strain, rotated, subjected to 100 strain cycles between 50% and 80%. (c) Profile delta field between uncycled, and cycled specimen scans.

Discussion

Analysis of polymer matrix composites with conductive inclusions often uses percolation theory to describe the increase in resistance due to applied strain(59, 60). As the material elongates, Poisson effects increase the volume of the polymer matrix by the relationship $V/V_0 = (1+\varepsilon)(1-\nu\varepsilon)^2$ where V and V_0 are final and initial volume, respectively, ε is applied macro strain, and ν is the Poisson ratio for the polymer matrix, presumed to be isotropic. By considering the inclusions to be rigid and undeformed, the change in matrix volume due to elongation reduces the overall volume fraction of the inclusions, causing a decrease in conductivity. Cracking is not considered in percolation models, even in higher order ones where the flakes are allowed to deform, which explains their poor correlation to measured results in

previous work. The cracking within PE 874 is a significant contributor to electrical performance degradation with monotonic strain(44), and necessitates a departure from the standard percolation theory. Cracks reduce the effective cross-sectional area of the conducting line, much like in metallic films. Unlike in metallic films, however, resistance is still measurable once these networks span the full width of the trace; the line remains conductive. This indicates that the crack channels formed during the initial elongation do not penetrate fully through the film thickness and only do so after repeated cycling.

From image analysis, crack density is found to remain constant, as no new channels are observed to form between 0 and 100 cycles. The topographical scans point to a deepening of existing cracks within the conductive ink is the primary response to strain cycling. When channel depth is sufficient to penetrate the thickness of the ink, it exhibits the open circuit result commonly observed in homogeneous metallic films. However, total film penetration is not expected to happen simultaneously for every channel. Rather it is a gradual process, whereby the first occurrence among cracks can be marked by the inflection point in the resistance evolution plot. As more cracks reach full depth with continued cycling, the instability in resistance measurement becomes more pronounced.

As the applied strain is decreased from maximum, electrical conductivity returns within the specimen. This may be because the decrease in the crack tip opening displacement can possibly restore some of the broken conductive paths along the crack faces. The reduction in the applied strain as ε_{min} is approached, decreases the crack tip opening displacement. We hypothesize that this decrease in the crack opening means that regions along the cracked surfaces can make contact. This renewed contact allows the conductive flakes to reconnect thereby decreasing the

resistance. Furthermore, the composite ink demonstrates a healing effect, whereby resistance recovery occurs even at constant strain. Each successive round of 10 cycles applied to the sample under the confocal microscope was preceded by a period of decreasing resistance. This is likely driven by time dependent properties of the film, whereby internal stress relaxation allows for reorientation of the conductive inclusions, and the formation of new percolative pathways.

Conclusions

This work examined the behavioral response of PE874 conductive ink when subjected to high strain cycling. Surface cracks are created during initial elongation to ε_{max} forming an interconnected network of surface cracks. The hybrid conductive ink traces continue to remain electrically conductive for multiple cycles despite the presence of such defects. Performance failure comes from the deepening of these cracks to full film thickness. Crack deepening is affected by strain amplitude. At low enough strain amplitudes, the mean strain also impacts the ink performance. The strain life curves over the full range of applied strains where PE874 is expected to operate can provide invaluable to design of devices for structural and health monitoring. Composite inks of the same class as PE874, can surprisingly remain conductive for multiple cycles despite appearance and subsequent deepening of cracks that form during the first initial loading.

Future work will need to explore more closely the driving mechanism behind the deepening of the cracks in PE874, and similar composite materials which exhibit such behavior. Polymer matrix failure due to fatigue, delamination between flakes and the matrix, or a combination of the two, are likely at play. Incorporation of in situ SEM into the experimental process would aid in this study.

Acknowledgements

The authors gratefully acknowledge funding support from the National Science Foundation (NSF CMMI-MOMS: 2026936). The authors are grateful to DuPont colleagues (Jeff Meth, Lynne Dellis and Augustus Jones) for providing samples.

Conflicts of Interest

The authors declare no conflicts of interest.

References

1. Dang WT, Vinciguerra V, Lorenzelli L, Dahiya R. Printable stretchable interconnects. Flex Print Electron. 2017;2(1).
2. McCoul D, Hu WL, Gao MM, Mehta V, Pei QB. Recent Advances in Stretchable and Transparent Electronic Materials. Adv Electron Mater. 2016;2(5).
3. Yao S, Zhu Y. Nanomaterial-Enabled Stretchable Conductors: Strategies, Materials and Devices. Advanced Materials. 2015;27(9):1480-511.
4. Kamyshny A, Magdassi S. Conductive nanomaterials for 2D and 3D printed flexible electronics. Chemical Society Reviews. 2019;48(6):1712-40.
5. Katsarelis C, Glushko O, Tonkin C, Kennedy MS, Cordill MJ. Crack Initiation of Printed Lines Predicted with Digital Image Correlation. Jom. 2018;70(9):1805-10.
6. Wyss A, Sologubenko AS, Mishra N, Gruber PA, Spolenak R. Monitoring of stress-strain evolution in thin films by reflection anisotropy spectroscopy and synchrotron X-ray diffraction. Journal of Materials Science. 2017;52(11):6741-53.
7. Glushko O, Klug A, List-Kratochvil EJW, Cordill MJ. Monotonic and cyclic mechanical reliability of metallization lines on polymer substrates. Journal of Materials Research. 2017;32(9):1760-9.
8. Kim BJ, Shin HAS, Lee JH, Yang TY, Haas T, Gruber P, et al. Effect of film thickness on the stretchability and fatigue resistance of Cu films on polymer substrates. Journal of Materials Research. 2014;29(23):2827-34.
9. Lambricht N, Pardoen T, Yunus S. Giant stretchability of thin gold films on rough elastomeric substrates. Acta Materialia. 2013;61(2):540-7.
10. Sim GD, Won S, Jin CY, Park I, Lee SB, Vlassak JJ. Improving the stretchability of as-deposited Ag coatings on poly-ethylene-terephthalate substrates through use of an acrylic primer. Journal of Applied Physics. 2011;109(7):5.
11. Lu NS, Suo ZG, Vlassak JJ. The effect of film thickness on the failure strain of polymer-supported metal films. Acta Materialia. 2010;58(5):1679-87.
12. Lu NS, Wang X, Suo ZG, Vlassak J. Failure by simultaneous grain growth, strain localization, and interface debonding in metal films on polymer substrates. Journal of Materials Research. 2009;24(2):379-85.
13. Lu NS, Wang X, Suo ZG, Vlassak J. Metal films on polymer substrates stretched beyond 50%. Appl Phys Lett. 2007;91(22):3.
14. Ibru T, Kalaitzidou K, Baldwin JK, Antoniou AJSm. Stress-induced surface instabilities and defects in thin films sputter deposited on compliant substrates. 2017;13(22):4035-46.
15. Harris K, Elias A, Chung H-J. Flexible electronics under strain: a review of mechanical characterization and durability enhancement strategies. Journal of materials science. 2016;51(6):2771-805.
16. Ou X-L, Feng J, Xu M, Sun H-B. Semitransparent and flexible perovskite solar cell with high visible transmittance based on ultrathin metallic electrodes. Optics Letters. 2017;42(10):1958-61.
17. Fan F-R, Tian Z-Q, Wang ZL. Flexible triboelectric generator. Nano energy. 2012;1(2):328-34.
18. Kim J, Wang Z, Kim WS. Stretchable RFID for wireless strain sensing with silver nano ink. IEEE Sensors Journal. 2014;14(12):4395-401.
19. Khan Y, Garg M, Gui Q, Schadt M, Gaikwad A, Han D, et al. Flexible hybrid electronics: Direct interfacing of soft and hard electronics for wearable health monitoring. Advanced Functional Materials. 2016;26(47):8764-75.
20. Claramunt S, Monereo O, Boix M, Leghrib R, Prades J, Cornet A, et al. Flexible gas sensor array with an embedded heater based on metal decorated carbon nanofibres. Sensors and Actuators B: Chemical. 2013;187:401-6.

21. Lee J, Kim S, Lee J, Yang D, Park BC, Ryu S, et al. A stretchable strain sensor based on a metal nanoparticle thin film for human motion detection. Nanoscale. 2014;6(20):11932-9.
22. Segev-Bar M, Haick H. Flexible sensors based on nanoparticles. ACS nano. 2013;7(10):8366-78.
23. Wagner S, Bauer S. Materials for stretchable electronics. Mrs Bulletin. 2012;37(3):207-13.
24. Liang JJ, Li L, Tong K, Ren Z, Hu W, Niu XF, et al. Silver Nanowire Percolation Network Soldered with Graphene Oxide at Room Temperature and Its Application for Fully Stretchable Polymer Light-Emitting Diodes. Acs Nano. 2014;8(2):1590-600.
25. Lee P, Ham J, Lee J, Hong S, Han S, Suh YD, et al. Highly Stretchable or Transparent Conductor Fabrication by a Hierarchical Multiscale Hybrid Nanocomposite. Adv Funct Mater. 2014;24(36):5671-8.
26. Chun KY, Oh Y, Rho J, Ahn JH, Kim YJ, Choi HR, et al. Highly conductive, printable and stretchable composite films of carbon nanotubes and silver. Nature Nanotechnology. 2010;5(12):853-7.
27. Lipomi DJ, Bao Z. Stretchable, elastic materials and devices for solar energy conversion. Energy & Environmental Science. 2011;4(9):3314-28.
28. Almusallam A, Yang K, Zhu D, Torah R, Tudor J, Beeby S, editors. Development of a low temperature PZT/polymer paste for screen printed flexible electronics applications. SENSORS, 2014 IEEE; 2014: IEEE.
29. Chamankar N, Khajavi R, Yousefi AA, Rashidi A, Golestanifard F. A flexible piezoelectric pressure sensor based on PVDF nanocomposite fibers doped with PZT particles for energy harvesting applications. Ceramics International. 2020;46(12):19669-81.
30. Sumita M, Sakata K, Asai S, Miyasaka K, Nakagawa H. Dispersion of fillers and the electrical conductivity of polymer blends filled with carbon black. Polymer bulletin. 1991;25(2):265-71.
31. Song P, Song J, Zhang Y. Stretchable conductor based on carbon nanotube/carbon black silicone rubber nanocomposites with highly mechanical, electrical properties and strain sensitivity. Composites Part B: Engineering. 2020;191:107979.
32. Jung YJ, Kar S, Talapatra S, Soldano C, Viswanathan G, Li X, et al. Aligned carbon nanotube–polymer hybrid architectures for diverse flexible electronic applications. Nano letters. 2006;6(3):413-8.
33. Mora A, Verma P, Kumar S. Electrical conductivity of CNT/polymer composites: 3D printing, measurements and modeling. Composites Part B: Engineering. 2020;183:107600.
34. Gbaguidi A, Madiyar F, Kim D, Namilae S. Multifunctional inkjet printed sensors for MMOD impact detection. Smart Materials and Structures. 2020;29(8):085052.
35. Pandhi T, Chandnani A, Subbaraman H, Estrada D. A Review of Inkjet Printed Graphene and Carbon Nanotubes Based Gas Sensors. Sensors-Basel. 2020;20(19):5642.
36. Merilampi S, Laine-Ma T, Ruuskanen P. The characterization of electrically conductive silver ink patterns on flexible substrates. Microelectronics reliability. 2009;49(7):782-90.
37. Liu X, Lei Z, Lin Z, Hu Y, Zhu P, Sun R, editors. Stretchable and Printable Conductive Polymer Composites for Electromagnetic Interference (EMI) Shielding Meshes. 2020 21st International Conference on Electronic Packaging Technology (ICEPT); 2020 12-15 Aug. 2020.
38. Araki T, Nogi M, Suganuma K, Kogure M, Kirihara O. Printable and stretchable conductive wirings comprising silver flakes and elastomers. IEEE Electron Device Letters. 2011;32(10):1424-6.
39. Mamunya YP, Davydenko VV, Pissis P, Lebedev EV. Electrical and thermal conductivity of polymers filled with metal powders. European Polymer Journal. 2002;38(9):1887-97.
40. Kim Y, Zhu J, Yeom B, Di Prima M, Su X, Kim J-G, et al. Stretchable nanoparticle conductors with self-organized conductive pathways. Nature. 2013;500:59.
41. Matos MAS, Tagarielli VL, Pinho ST. On the electrical conductivity of composites with a polymeric matrix and a non-uniform concentration of carbon nanotubes. Composites Science and Technology. 2020;188:108003.
42. Gong S, Zhu ZH. On the mechanism of piezoresistivity of carbon nanotube polymer composites. Polymer. 2014;55(16):4136-49.

43. Gbaguidi A, Namilae S, Kim D. Stochastic percolation model for the effect of nanotube agglomeration on the conductivity and piezoresistivity of hybrid nanocomposites. Computational Materials Science. 2019;166:9-19.
44. Cahn G, Barrios A, Graham S, Meth J, Antoniou A, Pierron O. The role of strain localization on the electrical behavior of flexible and stretchable screen printed silver inks on polymer substrates. Materialia. 2020:100642.
45. Lall P, Goyal K, Leever B, Miller S, editors. Reliability of Additively Printed Traces on Polymer Substrates Subjected to Mechanical Stretching. 2019 18th IEEE Intersociety Conference on Thermal and Thermomechanical Phenomena in Electronic Systems (ITherm); 2019: IEEE.
46. Garakani B, Sandakelum Somarathna KU, Weerawarne DL, Poliks MD, Alizadeh A, editors. Reliability of screen-printed conductors and resistors during fatigue cycling on flexible substrate. International Symposium on Microelectronics; 2019: International Microelectronics Assembly and Packaging Society.
47. Paul G, Torah R, Yang K, Beeby S, Tudor J. An investigation into the durability of screen-printed conductive tracks on textiles. Measurement Science and Technology. 2014;25(2):025006.
48. Happonen T, Häkkinen J, Fabritius T. Cyclic bending reliability of silk screen printed silver traces on plastic and paper substrates. IEEE Transactions on Device and Materials Reliability. 2015;15(3):394-401.
49. Araki T, Sugahara T, Nogi M, Suganuma K. Effect of void volume and silver loading on strain response of electrical resistance in silver flakes/polyurethane composite for stretchable conductors. Japanese Journal of Applied Physics. 2012;51(11S):11PD01.
50. Harea E, Datta S, Stěnička M, Stoček R, editors. Undesirable Aspects of Fatigue on Stretchable Elastomer Sensors2020; Dordrecht: Springer Netherlands.
51. Kim B-J, Haas T, Friederich A, Lee J-H, Nam D-H, Binder JR, et al. Improving mechanical fatigue resistance by optimizing the nanoporous structure of inkjet-printed Ag electrodes for flexible devices. Nanotechnology. 2014;25(12):125706.
52. Kim BJ, Cho Y, Jung MS, Shin HAS, Moon MW, Han HN, et al. Fatigue-Free, Electrically Reliable Copper Electrode with Nanohole Array. Small. 2012;8(21):3300-6.
53. DuPont. Dupont PE873 Stretchable Silver Conductor. Dupont; 2014. p. 1-2.
54. DuPont. Dupont Intexar TE-11C Base Film For Wearables Applications. 2017:1-2.
55. Scientific L. TST350 Temperature Controlled Tensile Stress Testing Stage: User Guide [Available from: https://static1.squarespace.com/static/556d800ae4b0e8f91507450c/t/56cf394886db43237cbed222/1456421216282/TST350_T95_manual.pdf.
56. Sim GD, Hwangbo Y, Kim HH, Lee SB, Vlassak JJ. Fatigue of polymer-supported Ag thin films. Scripta Materialia. 2012;66(11):915-8.
57. Leterrier Y, Mottet A, Bouquet N, Gilliéron D, Dumont P, Pinyol A, et al. Mechanical integrity of thin inorganic coatings on polymer substrates under quasi-static, thermal and fatigue loadings. Thin Solid Films. 2010;519(5):1729-37.
58. Blaber J, Adair B, Antoniou A. Ncorr: Open-Source 2D Digital Image Correlation Matlab Software. Experimental Mechanics. 2015;55(6):1105-22.
59. Last B, Thouless D. Percolation theory and electrical conductivity. Physical review letters. 1971;27(25):1719.
60. Shklovskiĭ B, Efros A. Percolation theory and conductivity of strongly inhomogeneous media. Soviet Physics Uspekhi. 1975;18(11):845.